# How Many Maps are there in Visual Cortex?

Nicholas V. Swindale

Department of Ophthalmology, University of British Columbia, 2550 Willow Street, Vancouver, BC, Canada V5Z 3N9

**In addition to a topographic map of the retina, mammalian visual cortex contains superimposed, orderly periodic maps of features such as orientation, eye dominance, direction of motion and spatial frequency. There is evidence that these maps are overlaid so as to ensure that all combinations of the different parameters are represented as uniformly as possible across visual space. However, it is unknown to what extent geometrical factors limit the number of periodic maps which might simultaneously be present, given this constraint. This paper attempts to investigate the question by using a dimension reduction model to generate maps of simple, many-dimensional feature spaces onto a model two-dimensional cortex. The feature space included a model retina, plus *N* binary variables, corresponding to parameters such as ocular dominance or spatial frequency. The results suggest that geometrical factors do not sharply limit the ability of the cortex to represent combinations of parameters in spatially superimposed maps of similar periodicity. Considerations of uniform coverage suggest an upper limit of six or seven maps. A higher limit, of about nine or ten, may be imposed by the numbers of neurons (or minicolumns) available to represent each of $2^N$ features within a given small region of cortex.**

## Introduction

Anatomical and physiological studies have shown that, in addition to a topographic map of the retina, mammalian primary visual cortex contains superimposed, orderly periodic representations, or maps, of different visual feature attributes. In many species, including primates, these representations include line orientation (Hubel and Wiesel, 1974; Blasdel and Salama, 1986) and the eye in which the stimulus is present (or ocular dominance) (Hubel *et al.*, 1977). In the visual cortex of cats and ferrets, there are, in addition to maps of orientation and eye dominance, maps for direction of motion (Shmuel and Grinvald, 1996; Weliky *et al*., 1996) and spatial frequency (Hübener *et al*., 1997; Shoham *et al*., 1997).

Hubel and Wiesel suggested that orientation and ocular dominance maps might be overlaid in such a way as to optimize the uniform representation of all possible combinations of orientation, eye of origin and retinal position (Hubel and Wiesel, 1977). One way of ensuring this would be for iso-orientation domains and ocular dominance stripes to intersect at right angles. Such a relationship has been observed experimentally in primates (Bartfeld and Grinvald, 1992; Obermayer and Blasdel, 1993). In cat area 17, optical recording experiments have shown that three stimulus features – orientation, eye of origin and spatial frequency – are represented in superimposed, spatially periodic maps (Hübener *et al.*, 1997). Analysis of these maps suggests that the geometrical relations between orientation, ocular dominance and spatial frequency maps are such as to optimize the uniform representation across the retina of each possible combination of the three feature variables (N.V. Swindale, D. Shoham, A. Grinvald, T. Bonhoeffer and M. Hübener, submitted). It is possible that similar constraints might apply not just to primary visual cortex but to the organization of higher-level feature maps in other visual cortical areas (Felleman and Van Essen, 1991) and to auditory cortex, where there is also evidence for superimposed feature maps (Langner *et al.*, 1997; Schreiner, 1998).

Given these findings, it is natural to ask whether or not maps of additional, as yet unknown, features are represented in spatially periodic maps in the visual cortex. The list of possible features is potentially long, and, in the cat, might include selectivity for edge curvature (Dobbins *et al.*, 1987), positional disparity (Barlow *et al.*, 1967), orientation disparity (Nelson *et al.*, 1977), receptive field phase (Tanaka, 1995), preferred temporal frequency and response latency (De Angelis *et al.*, 1999). Although only experiments can determine which properties have a spatially periodic representation, it may be useful to investigate the factors limiting the numbers of maps from a modelling perspective. Questions that can be asked include: (i) Are there limits on the number of stimulus features (or dimensions) that can be overlaid in such a way that each is continuous and periodic, and so that all combinations of the different features occur with reasonably equal frequency across the retinotopic map? (ii) Does the structure of individual maps change as new maps are added? (iii) Do the structural relations between different maps change as new maps are added? (iv) If they do, is there any way one can tell, from looking at maps of individual features, how many additional features might be represented in a similar way within the same cortical region?

I have attempted to answer these questions by using the Kohonen self-organizing feature map (SOFM) algorithm (Kohonen, 1982) to generate maps of simple, many-dimensional feature spaces onto a model two-dimensional visual cortical surface. Previous studies (Obermayer *et al.*, 1990, 1992; Goodhill, 1993; Wolf *et al.,* 1994; Swindale and Bauer, 1998) have shown that the SOFM algorithm is able to produce mappings that bear a detailed resemblance to real visual cortex maps. The feature space studied here included a model retina (i.e. two continuous dimensions), plus the vertices of an *N*-dimensional hypercube (i.e. binary variables corresponding to parameters such as ocular dominance or spatial frequency domains).

The maps, produced by simulations done with values of *N* in the range 2–9, were analysed with respect to (i) the periodicity and orderliness of the stripe patterns that were formed; (ii) the positions of the intersections of the stripe boundaries (i.e. zero crossings) of pairs of patterns and the angles at which the boundaries intersect; (iii) coverage uniformity (Swindale, 1991) i.e. the uniform distribution across the cortex of each combination of features; and (iv) the degree of disorder in the retinotopic map.

The results suggest that it may not be straightforward to tell, from looking at one or a small number of individual maps, how

many additional maps might be represented. Nor does it appear that geometrical factors on their own sharply limit the ability of the cortex to represent combinations of parameters in spatially superimposed, periodic, stripe-like maps, at least up to about six or seven maps. A higher limit, of about nine or ten, may however be imposed by the numbers of neurons (or mini-columns) available to represent each of $2^N$ features within a given small region of cortex.

## Methods

### *Simulation Details*

Kohonen's SOFM algorithm (Kohonen, 1982) was used to generate the maps, partly because of its computational simplicity and partly because of its ability to reproduce the biological details of real visual cortex maps in other situations. Other algorithms (or developmental models) might in principle be used for the same purpose and might produce different solutions to the same mapping problem. This possible restriction on the results will be discussed later.

Following earlier work (Obermayer *et al.*, 1990; Swindale and Bauer, 1998), the algorithm was applied in the following way: first define a Euclidian stimulus space, consisting of two retinal dimensions (the horizontal and vertical components of receptive field position) plus $N$ additional dimensions. The model cortex is represented as a two-dimensional grid of points, indexed by $i$ and $j$, lying within the stimulus space. The position of each cortical point in the space defines the set of stimulus values assigned to it i.e. its receptive field. This is given by $\mathbf{w}_{i,j} = (x, y, a_1, a_2, \ldots, a_N)$ where $x$ and $y$ are the retinal position of the receptive field of the point $(i,j)$ and $a_1$, $a_2$, etc., are the values of the additional stimulus dimensions assigned to it. 'Stimuli', defined by the vector $\mathbf{v} = (x_s, y_s, b_1, b_2, \ldots, b_N)$, are chosen one at a time, usually at random from a subset of points in the space. For each, the nearest cortical point is found; this point, and surrounding ones defined by a circular neighbourhood function, are then moved closer towards the stimulus. Physiological interpretations of this learning rule have been given elsewhere (Kohonen, 1993; Kohonen and Hari, 1999).

After each presentation of a stimulus vector $\mathbf{v}$, cortical receptive fields change by an amount

$$\Delta w_{i,j} = \varepsilon h(\mathbf{r})(\mathbf{v} - \mathbf{w}_{i,j}) \quad (1)$$

where $\varepsilon$ is a rate constant, $\mathbf{r}$ is the distance the between the cortical point nearest the stimulus and point $(i,j)$, and $h(\mathbf{r})$ is a neighbourhood function given by

$$h(\mathbf{r}) = \exp(-|\mathbf{r}|^2/2\sigma_c^2) \quad (2)$$

where $\sigma_c$ is a width parameter. Two sets of simulations were done: one in which the value of $\sigma_c$ remained constant, and another in which $\sigma_c$ was slowly reduced in size, to a lower minimum, a process referred to as annealing. Details of how this was done are given below.

In the simulations presented here the cortex was represented by an $M \times M$ grid of points with values $x_{i,j}$, $y_{i,j}$, $a_{1i,j}$, etc. where $i,j = 0, 1, \ldots, M-1$. Initially a roughly ordered receptive field topography was assumed to be present, with $x_{i,j} = iX/(M-1) + \xi_x$ and $y_{i,j} = jY/(M-1) + \xi_y$ where $\xi_x$ and $\xi_y$ are random numbers drawn from a Gaussian distribution with a mean of zero and a standard deviation = $\sigma_r$. $X$ and $Y$ give the overall (fixed) extent of the region of retina mapped onto the cortex. The initial values of $a_{1,i,j}$, $a_{2,i,j}$ etc. were also Gaussian random numbers with a mean of zero and standard deviation = $\sigma_a$.

Stimuli were calculated as follows: retinal position values $x_s$ and $y_s$ were chosen with uniform probability in the intervals $[0,X]$ and $[0,Y]$ respectively. The values of $b_1$, $b_2$, etc., were each set equal to +1 or –1 with equal probability. The procedures *ran1* and *gauss* (Press *et al.*, 1994) were used to generate the random numbers.

### *Terminology*

Following Landau and Schwartz (Landau and Schwartz, 1991) and to avoid confusion about the meaning of the word 'map', the term 'protomap' will be used to refer to the mapping of one of the $N$ possible dimensions, i.e. the values of $a_1$, or of $a_2$, etc. The complete set of $N$ such maps, i.e. for $a_1 \ldots a_N$ will be termed a 'polymap'. In cases where there is no ambiguity, the term 'map' will either refer to an individual map (i.e. a protomap) or to the complete set of maps (a polymap). Although the values of $a_i$ are continuous, for the most part they will be treated as if they were binary variables, i.e. only the sign of $a_i$ is taken into account. A unique combination of binary values, of which there are $2^N$ , will be termed a 'feature' (i.e. a specific combination of the lower-level features represented in the protomaps). A spatially contiguous region of cortical points with the same feature value will be termed a 'feature domain'.

### *Parameter Values*

In all the simulations, $M$ =150, $\varepsilon$ = 0.01, $\sigma_r$ = 0.1, $\sigma_a$ = 0.1 and the total number of stimuli given was $2.5 \times 10^6$. This corresponds to about 111 stimuli per cortical array point. The choice of when to stop a simulation is somewhat arbitrary, but was governed by the length of computer time required (typically several hours for each map) and the fact that by this point map structure is changing at a very slow rate. These continued slow changes included an increase in the spatial wavelength of the protomaps, and a decline (at an exponentially decreasing rate) in coverage values. Compared with the impact of $N$, however, these changes were small. In one set of simulations, denoted 'no annealing', the cortical neighbourhood function, $\sigma_c$, was kept constant in size, at 2.5 array units, and the size of the 'retina' was $X = Y = 6.0$. In a second set of simulations (annealing), $\sigma_c$ was kept constant at 2.5 for the first $10^6$ stimulus presentations, and was then gradually reduced in size by multiplying by 0.999 every $10^3$ stimuli. When it reached a lower limit of 1.0 (after about a further $9 \times 10^5$ stimuli) $\sigma_c$ was kept constant for the remaining stimulus presentations (approximately $6 \times 10^5$). For these simulations the size of the 'retina' was $X = Y = 5.0$. This was done in order to make the spatial wavelengths of the protomaps similar in the annealed and non-annealed cases. Annealing tends to reduce the spatial wavelength of the protomaps and increasing the size of the retina offsets this effect.

Assuming that the protomap wavelength (typically around 28 pixel units: see Fig. 2*a*) corresponds to a distance of 1 mm in the real cortex, the cortical array units in the simulations have a spacing of ~36 μm, which corresponds roughly to the size of a cortical 'minicolumn' (Mountcastle, 1978). Thus, the granularity of the simulations corresponds, at least approximately, to the granularity of the real cortex.

As described below, the number of dimensions, $N$, was varied between 2 and 9. For each value of $N$, three separate polymaps were generated using a different initial random number seed for each.

Maps were analysed with respect to pattern periodicity, pattern morphology, coverage uniformity, zero-crossing intersection angle, the spatial distribution of zero-crossing intersections and retinotopy. The methods used to do each type of analysis are described as follows.

### *Periodicity*

The Fourier power spectra of the protomaps were annular in shape, with energy spread over a large number of local peaks at different orientations but similar distances from the origin. This is consistent with the visual appearance of a periodically striped pattern with no predominant orientation. Periodicity was measured by estimating the average radial distance of the peak in the annulus from the origin. This was done by calculating a least-squares fit of a model function to the two dimensional power spectrum. The model function, defined in polar coordinates $(r,\theta)$ was the product of a Gaussian function of $r$ and a circular normal distribution (a von Mises function) of $\theta$, i.e.

$$E(r,\theta) = E_{\max} e^{-(r-r_0)^2/2\sigma_E^2} \cdot e^{k\left[\cos 2(\theta-\theta_0)-1\right]} \quad (3)$$

where $E$ is the energy in the power spectrum at position $(r,\theta)$, $E_{\max}$ is the maximum amplitude, $r_0$ is the peak spatial frequency, $\theta_0$ is the angle made by the peak with the origin, and $\sigma_E$ and $k$ measure the spread of energy in the radial and angular dimensions respectively. Parameter $k$ measures spatial anisotropy in the pattern of stripes: if it is small, energy is distributed over a wide range of angles, and there is no predominant stripe orientation in the pattern. If the value is large, then the pattern is anisotropic, in which case $\theta_0$ gives the orientation orthogonal to that in which the stripes tend to run.

**Table 1**
Summary of mathematical symbols

| Symbol | Meaning | Value |
|---|---|---|
| *Model parameters* | | |
| $a_n$ | cortical feature value for the *n*th map | |
| $b_n$ | stimulus feature value for the *n*th map | ±1 |
| ε | learning rate | 0.01 |
| $h(r)$ | rate of learning as a function of cortical distance *r* from maximally responsive cortical point (cortical neighbourhood function) | |
| $i,j$ | indexes to points on the two-dimensional cortical grid | |
| $N$ | number of cortical maps, excluding the retina | 2–9 |
| $M$ | size of model cortex in pixel units | 150 |
| $\sigma_a$ | initial standard deviation of cortical feature values | 0.1 |
| $\sigma_c$ | width of cortical neighbourhood function in pixel units | ≤2.5 |
| $\sigma_r$ | initial standard deviation of retinotopic map from uniform linear projection in degrees | 0.1 |
| $\mathbf{v}$ | stimulus feature vector | |
| $\mathbf{w}_{i,j}$ | feature vector, i.e. receptive field, mapped to cortical point $(i,j)$ | |
| $x_{i,j}, y_{i,j}$ | position in retinal space of point $(i,j)$ in degrees | |
| $X,Y$ | size of model retina in degrees | 5 or 6 |
| *Analysis parameters* | | |
| $A$ | total cortical activity in response to a stimulus | |
| $c'$ | coverage uniformity | |
| $c_2$ | measure of coverage based on feature domain spacing | |
| $E(r,\theta)$ | energy in the power spectrum of a protomap pattern | |
| $d_{i,j}$ | deviation in degrees of point $(i,j)$ from a uniform linear retinal map | |
| $f(x,y,\ldots)$ | receptive field of a cortical unit | |
| $g(a)$ | response of cortex as a function of binary feature variable | |
| $k$ | estimate of angular dispersion of energy in the power spectrum | |
| λ | estimate of peak spatial wavelength of a pattern in pixel units | |
| Λ | total length of zero-crossings in a pattern in pixel units | |
| $m$ | total number of zero-crossing intersections in a polymap | |
| Ω | measure of spatial order in a periodic pattern | |
| $r_0$ | estimate of peak spatial frequency in a protomap pattern | |
| $r_m$ | radius of largest circular region not overlapping a specific feature domain | |
| $(r,\theta)$ | polar coordinates in frequency space | |
| $R$ | area of a protomap pattern in square pixels | |
| $s$ | measure of disorder in the retinotopic map | |
| $\sigma_E$ | estimate of radial dispersion of energy in the power spectrum | |
| σ | retinal receptive field size in degrees | |
| $\theta_0$ | angle made by peak in power spectrum w.r.t. the origin | |
| $(u_i,v_i)$ | position of *i*th zero-crossing intersection of a pair of protomaps | |

After calculating the power spectrum from a given pattern in a 256 × 256 array, Levenburg–Marquardt minimization (Press *et al.*, 1994) was used to find the best-fitting values of $E_{max}$, $r_0$, $\sigma_E$, $k$ and $\theta_0$. Peak spatial wavelength, λ, was then calculated as

$$\lambda = 256/r_0 \tag{4}$$

Simpler techniques, such as just taking the position of the maximum, or averaging across θ, and then estimating a maximum, proved to be less accurate, or unreliable when tested with patterns of known spatial periodicity. Nor did these obvious alternatives capture features such as the degree and direction of spatial anisotropy in the spectrum that might potentially be of interest.

### *Pattern Morphology*

Adding extra dimensions might be expected to produce increased spatial disorder in the protomaps. A simple dimensionless measure of spatial disorder, Ω, in a pattern $a_i$, which is independent of the spatial period, λ, is

$$\Omega = \Lambda\lambda/R \tag{5}$$

where Λ is the total length of the stripe edges (i.e. the zero-crossings in $a_i$) and $R$ is the total area containing the pattern. For a pattern with a fixed morphology, Ω and λ are independent: e.g. if a given pattern is expanded in size by a factor of 2, both the wavelength, λ and the edge length Λ, double, while the area increases by a factor of 4, leaving Ω unchanged. It is simple to show that for parallel stripes Ω = 2.0, which is probably the minimum possible value for a periodic pattern which subdivides a surface into two equal areas. For circles on a square lattice, Ω = 2.5, and for circles on a hexagonal lattice Ω ≈ 2.69.

The length of the stripe edges was calculated by subdividing the pixel grid into triangles defined by groups of three adjacent pixels. For each triangle, the equation of the plane $z(x,y) = m_1x + m_2y + c$ passing through all three pixels was calculated. If the straight line defined by $z = 0$ intersected the triangle, the length of the intersection was added to the total edge length. This was repeated for all the triangles in each pattern to find the total edge length.

### *Coverage Uniformity*

Coverage measures how well, or uniformly, a set of stimuli is represented within a map on the cortex. Adding extra stimulus dimensions to those that have orderly representations in a map might be expected to either degrade the spatial orderliness of the map, reduce the uniformity of the representation, or do both. Different measures of coverage were defined as follows:

Following Swindale (Swindale, 1991), for a stimulus $\mathbf{v}$, the total amount of activity, $A$, evoked in the cortex is given by

$$A(\mathbf{v}) = \sum_{i,j} f\left(\mathbf{v} - \mathbf{w}_{i,j}\right) \tag{6}$$

where $f$ is the receptive field of each cortical unit and the summation is over all the points in the cortex. Coverage uniformity is defined over a representative set of stimuli, and is given by

$$c' = \text{standard deviation}(A)/\text{mean}(A) \tag{7}$$

(or)

$$c' = \langle |A - \langle A\rangle|^2\rangle/\langle A\rangle \tag{7a}$$

For simplicity, $f$ was assumed to be given by

$$f(x,y,a_1,a_2,\ldots,a_N) = e^{-\left(x^2+y^2\right)/2\sigma^2} \prod_{n=1}^{N} g(a_n) \tag{8}$$

where

$$g(a) = \begin{cases} 1 \text{ if } -0.5 < a < 0.5 \\ \\ 0 \text{ otherwise} \end{cases}$$

and σ is the receptive field size in retinal coordinates. For the calculations, σ = 0.48. This corresponds approximately to a cortical point image diameter of 2.0 mm (Hubel and Wiesel, 1977), assuming a scaling of 28 pixels (the mean protomap wavelength) ≈ 1 mm of real cortex, and a retinal magnification = $X/M$ degrees/pixel.

A separate measure of coverage, which ignores the structure of the retinotopic map, was defined. This measure looks for 'holes' in the representation of specific feature domains in the map. For a given feature domain value, the radius $r_m$ of the largest circular region, lying entirely within the boundaries of the map, which did not overlap any of the specified feature domains, was found by iterative search. The average of this radius, taken over all $2^N$ features, was divided by the mean spatial wavelength $\langle\lambda\rangle_N$ of the protomaps to give a measure

$$c_2 = \frac{\langle r_m \rangle}{\langle \lambda \rangle_N} \tag{9}$$

Calculated values of $c_2$ can be compared with a notional 'ideal' situation, in which feature domains contrive to be circular and represented on a cubic lattice with a spacing λ. In this case the area of each domain = $\lambda^2/2^N$, and it is simple to show that

$$c_{2\text{ideal}} = \frac{r_m}{\lambda} = \frac{1}{\sqrt{2}}\left(1 - \frac{1}{\sqrt{2^{N-1}\pi}}\right) \tag{10}$$

***Zero-crossing Intersection Angle and Distribution of Intersection Points***

The spatial relationships between pairs of patterns were analysed by calculating the positions at which pairs of zero-crossings intersected, and the angle between the zero-crossings at the point of intersection. This was done for all pairs of maps in a given simulation. The positions of the intersections were calculated using the sub-pixel triangulation method described above.

Histograms of the intersection angles were compiled for points where only a single pair of zero-crossings intersected. These were defined as points of intersection where no other zero-crossing intersection between any pair of protomaps was within a distance of 2.5 pixel units from the crossing in question. Histograms were also compiled for points where only three zero-crossings intersected (yielding three points of intersection). A set of zero-crossings was considered to satisfy this arrangement if (i) a single intersection was found; (ii) two other intersection points were found within 1 pixel unit distance from the first intersection; (iii) no other intersection points occurred within a distance of 2.5 pixel units from the first point; and (iv) the three intersections were produced by three different protomaps.

For any zero-crossing intersection in a pair of maps, the probability of finding a second intersection in a pair of maps a given distance apart (the two-point autocorrelation function) was calculated. Let $(u_i,v_i)$ be the position of the $i$th zero-crossing intersection calculated for all possible pairs of maps and let $m$ be the total number of such intersections. Then

$$p(u,v) = \frac{\sum_{i\neq j}^{m}\sum_{j}^{m}\left(u_i - u_j, v_i - v_j\right)}{m(m-1)} \tag{11}$$

gives the probability of occurrence of a pair of intersections a given distance $(u,v)$ apart. For example, a peak close to the origin would indicate a tendency for intersections to cluster, i.e. for three or more zero-crossings to intersect at the same point. A peak at a given distance from the origin indicates a tendency for intersections to be spaced that distance apart.

***The Retinotopic Map***

The amount of disorder in the retinotopic map was calculated by first assuming that a perfectly ordered retinotopic map would correspond to one in which the horizontal and vertical components of retinal position are mapped linearly and orthogonally in the $i$ and $j$ directions respectively on the cortex, i.e. that

$$\bar{x}_{i,j} = iX/(M-1) \quad \text{and} \quad \bar{y}_{i,j} = jY/(M-1)$$

The deviation of a single point from this value is

$$d_{i,j} = \sqrt{\left(x_{i,j} - \bar{x}_{i,j}\right)^2 + \left(y_{i,j} - \bar{y}_{i,j}\right)^2}$$

and scatter, $s$, was measured as the r.m.s. value of $d$ taken over the whole map, i.e.

$$s = \frac{1}{M}\sqrt{\sum_{\text{map}} d_{i,j}^2} \tag{12}$$

The idea that the retinotopic map is in some sense a disorderly approximation to the ordered one defined in this way appears to be justified, because it was found that $\langle x_{i,j} - \bar{x}_{i,j}\rangle$ and $\langle y_{i,j} - \bar{y}_{i,j}\rangle$ were always close to zero and much smaller than the r.m.s. values.

## Results

### *Protomap Morphology*

Visual inspection of maps of individual feature dimensions (protomaps) suggests relatively little morphological change with the addition of extra dimensions (Fig. 1). In the non-annealed maps, the edges became more indistinct as $N$ increased, because of a greater number of points at the pattern borders with values of $a$ intermediate between the stimulus values of +1 and –1. Numerical analysis showed that $N$ had little impact on the pattern wavelength $\lambda$ in both the non-annealed and annealed cases (Fig. 2*a*). In the non-annealed cases the spatial disorder measure, $\Omega$ (eq. 5) was lowest for $N = 2$ but changed little over the range $N = 3$ to $N = 9$. Annealing resulted in larger values of $\Omega$ for all values of $N$. $\Omega$ increased over the range $N = 2$ to $N = 5$ but there was little indication of any further increase for $N > 5$ (Fig. 2*b*).

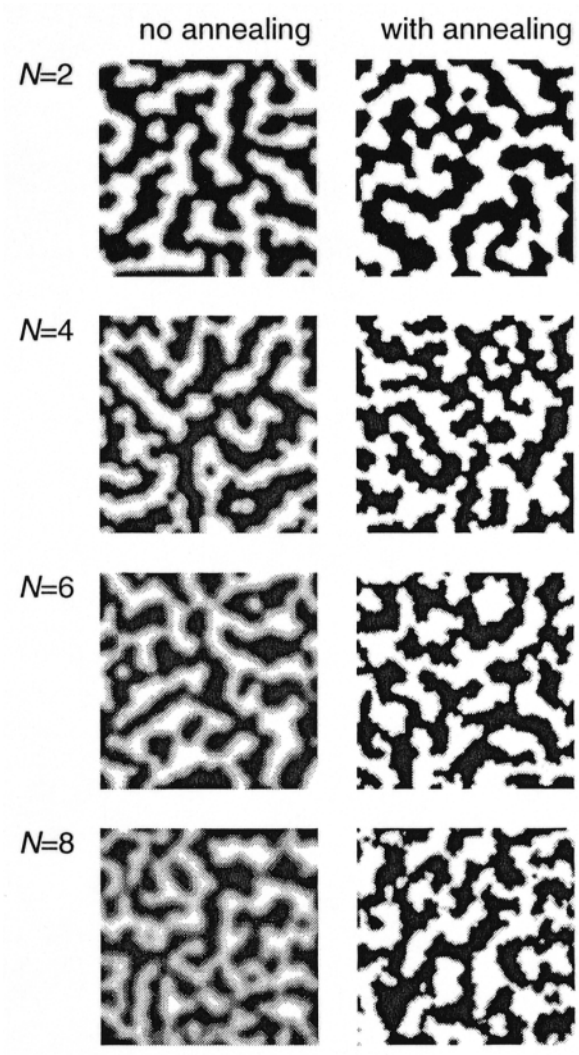


**Figure 1.** Examples of protomaps formed for hypercube mappings of different dimensionality, $N$. Only one out of the total of $N$ protomaps is shown in each case. Panels on the left are from maps where the size of the cortical neighbourhood function remained constant during development (no annealing); panels on the right are from simulations where the size was slowly reduced (annealing).

### *Zero-crossing Intersections*

For larger values of $N$, diagrams of superimposed sets of zero-crossings (i.e. stripe borders) revealed an arrangement, often reminiscent of Celtic braiding, in which the borders showed a tendency for parallel, equidistant, spacing as well as a bias towards orthogonal intersections (Fig. 3). Numerical

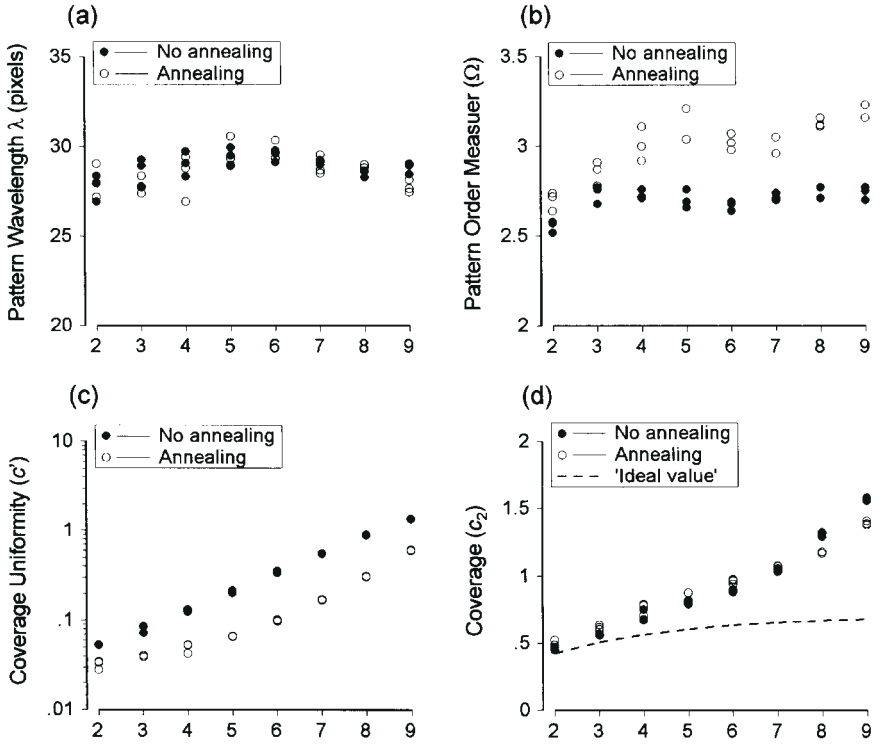


**Figure 2.** Graphs showing the effect of *N* (the number of feature dimensions, or protomaps, on the horizontal axes) on (*a*) the average spatial wavelength of the protomaps; (*b*) stripe morphology (measure Ω, eq. 5); (*c*) the coverage measure *c′* and (*d*) the coverage measure $c_2$. The dashed line in (*d*) shows the behaviour of the 'ideal' measure (eq. 10). Data points from three separate simulations for each value of *N*, for the non-annealed (filled circles) and annealed cases (open circles) are shown.

analysis of the intersection angles of pairs of zero-crossings (Fig. 4) showed the following: for $N \leq 4$ in the non-annealed case, and $N \leq 6$ in the annealed case, the distributions were strongly biased towards intersections at small angles. This implies a tendency, visually apparent in Figure 3, for zero-crossing borders to coincide and run parallel with each other over short distances. For $N \geq 5$ in the non-annealed case and $N \geq 7$ in the annealed case, there was a sharp transition to a bias towards orthogonal intersections. (Note that random intersections between spatially independent patterns will produce a cosine rather than a flat distribution.)

Visual inspection of zero-crossing patterns for $N \geq 6$ suggests that sets of three zero-crossings might have a tendency to intersect in the same place at an angle of ~60°. This was confirmed, but only in the non-annealed cases, for $N \geq 6$ (Fig. 4*a*). In the annealed cases the triplet intersection angles were, like those of the pairs, strongly biased towards small angles for $N \leq 6$. For $N = 7$ the distribution was flat, while for $N = 8$ and $N = 9$ it was approximately cosine in shape, which is consistent with a random relationship.

The probability of finding a pair of zero-crossing intersections a given distance apart (i.e. the two-point autocorrelation function: eq. 11) was calculated and plotted as a two-dimensional density function (Fig. 5). These plots, which were similar in the annealed and non-annealed cases, showed two main features: a central narrow peak (for $N > 2$) surrounded by an annular trough of decreased probability. A weak secondary annular peak of increased probability surrounding the trough was also visible for $N \geq 7$. The distance of this region from the origin, and that of the trough, decreased as *N* increased. The peak at the origin implies a strong tendency for more than two zero-crossings to intersect at the same location, i.e. a short-range attraction of intersection points while the annular trough and secondary peak imply a tendency for the points of intersection to be spaced a fixed distance apart, this distance decreasing, as might be expected, with increasing *N*.

The effect of these behaviours is to cause the polymap to be subdivided into small, often square-shaped, feature domains of roughly equal size. Each domain represents a particular combination of binary feature values, which can be represented as an *N*-bit binary number, giving $2^N$ possible combinations. The appearance and distribution of these domains can be represented in colour plots, with each colour representing a unique combination of features, i.e. a number in the range 0 to $2^N - 1$ (Fig. 6). It is useful to let each of the *N* dimensions correspond to a particular vector in colour space when constructing such plots, since the individual protomaps are then partly identifiable on the basis of colour.

### *Coverage Measures*

Calculations of the two coverage measures, *c′* (eq. 7) and $c_2$ (eq. 9), led to slightly different interpretations of the impact of *N*. On a log scale, *c′* increased linearly with *N* (Fig. 2*c*) in the non-annealed cases, with a slope of ~0.470. In the annealed cases values of *c′* were significantly smaller and also increased with *N*, with a slope of ~0.414.

The second measure of coverage, $c_2$ (Fig. 2*d*), increased approximately linearly with *N*, with a slightly larger rate of increase for $N \geq 7$, particularly in the non-annealed cases. As would be expected, $c_2$ is always larger than the ideal value. Annealing had relatively little impact on this measure of coverage, in contrast to its effects on *c′*.

While it is not possible to say what constitutes an acceptable upper limit for either *c′* or $c_2$, values of $c_2 > 1$ imply the relatively

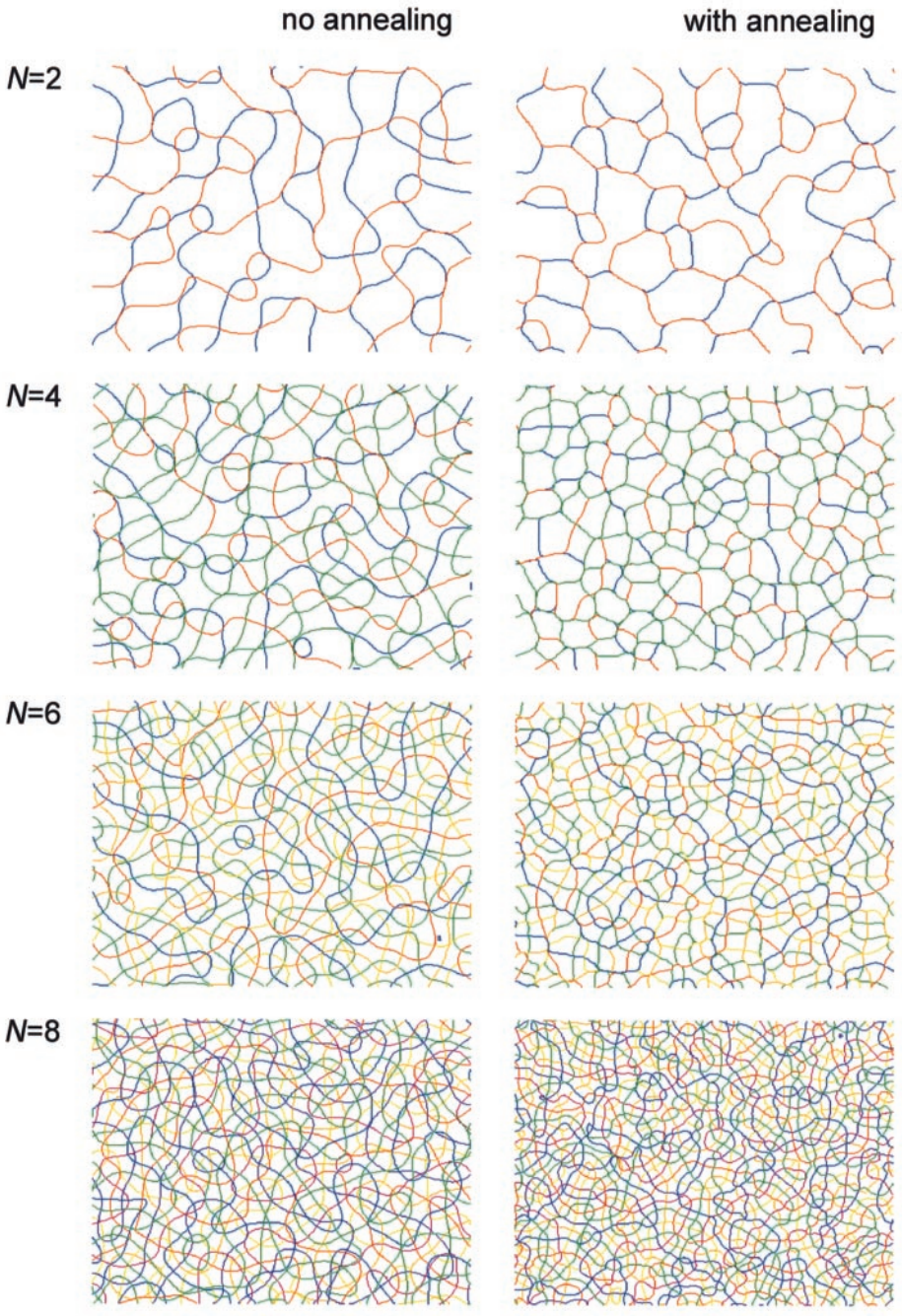


**Figure 3.** Arrangement of zero-crossing boundaries for different values of *N*. Specific protomaps are identified by the colour of their boundaries. Note the prevalence of orthogonal intersections at larger values of *N*, and, for $N > 2$, multiple crossings at the same position. The images are of regions approximately $103 \times 77$ array units in size.

frequent occurrence of regions with a diameter equal to twice the overall pattern spacing, in which particular feature domains fail to be represented. This might perhaps be regarded as a failure to meet the design consideration that 'all combinations of different features should occur with reasonably equal frequency across the map'. On the basis of this criterion, the upper limit on *N* might be about six or seven.

### *The Retinotopic Map*

Visual inspection of the retinotopic maps for the simple cases where $N = 1$ or $N = 2$ showed a correspondence between folds (or local distortions) and the zero-crossing borders of the protomaps. This correspondence was similar to that described for a related model (in which $N = 1$) by Goodhill (Goodhill, 1993). For larger values of *N* the retinal map was folded and distorted in a more complex way and it proved hard to discern a lawful relationship between the distortions and the organisation of the protomaps. Figure 7*a* shows how the r.m.s. deviation between actual receptive field position and the position expected on the basis of a uniform retinotopic mapping (eq. 12) varies with *N*. Measured this way, the deviation of the retinotopic map from uniformity tends to increase with increasing *N*: for the

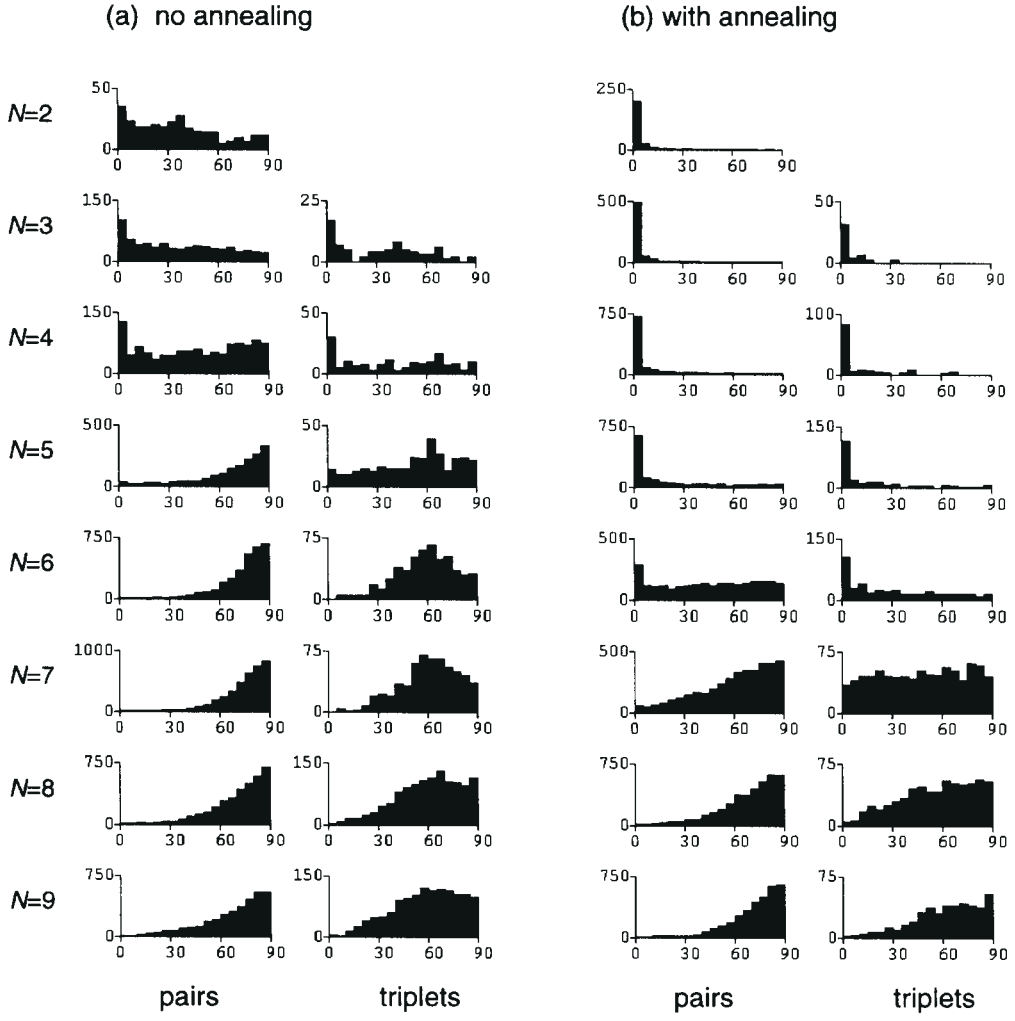


**Figure 4.** Histograms showing the relative prevalence of angles at which zero-crossings (protomap domain boundaries) intersect, for different values of *N*. The histograms in (*a*) are from maps where the size of the cortical neighbourhood function remained constant in size during development (no annealing) and the histograms in (*b*) are from simulations where the size was slowly reduced (annealing). Histograms in the columns labelled 'pairs' are for points where only two zero-crossings intersect; those in columns labelled 'triplets' are for regions where three zero-crossings intersect close together. Each histogram is the sum of those obtained from three separate polymap simulations and the bins are 5° wide.

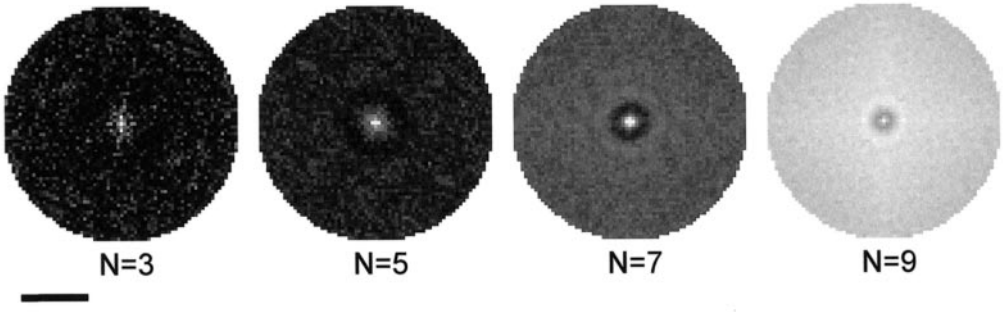


**Figure 5.** Plots showing the relative probability (eq. 11) of finding two zero-crossing intersections (from the same or a different pair of maps) a given distance apart, for different values of *N*. Zero separation is at the centre of each plot. Thus the bright peak at the centre of the plots indicates a tendency for the zero-crossings of different protomaps to intersect at the same location. Each plot is the average obtained from three separate polymap simulations, for the annealed case. Results from the non-annealed polymaps were similar. The scale bar is about 10 array units long.

non-annealed cases the deviations are smaller, and may reach an upper limit for $N \geq 7$; for the annealed cases, the values reach a maximum at $N = 5$ or $N = 6$, and then tend to decline. Figure 7*b* shows a representative example of a retinotopic mapping, for $N = 7$ in the non-annealed case. The lattice of points represents the cortical array, with position on the page corresponding to retinal position. The representation of retinal position in the cortical map is non-uniform, with some retinal regions being

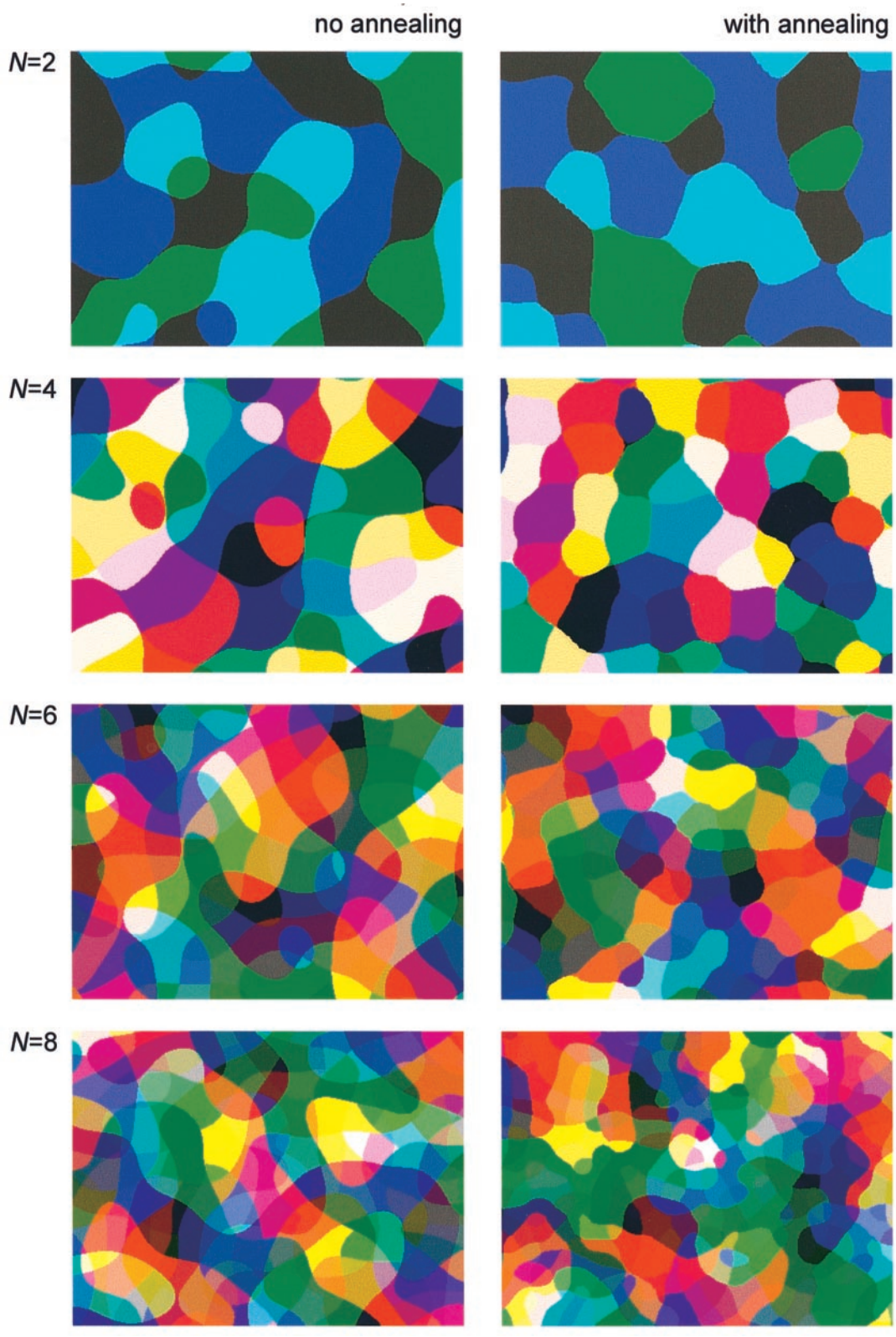


**Figure 6.** Feature domain maps for different values of $N$. Each feature domain (of which there are $2^N$ possible types for a given polymap) is represented by a unique colour. Regions shown are 60 × 45 array units in size.

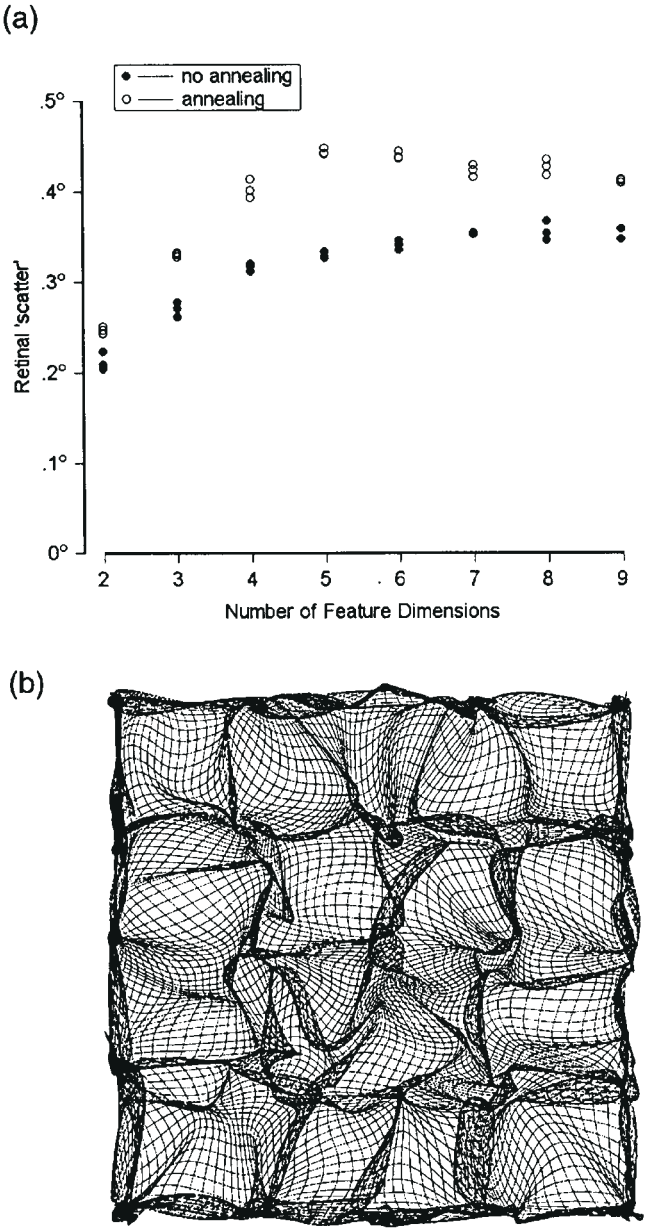


**Figure 7.** (*a*) Graph showing the r.m.s. deviation of the retinotopic map from a perfectly uniform map (eq. 12), for different values of *N* in the non-annealed and annealed cases. Each point is from a single polymap. (*b*) Example showing a projection of the cortex into retinotopic space for a polymap where $N = 7$ (no annealing): each lattice point is a single point in the cortical array, and position on the page is equivalent to position in retinal space. The representation of retinal position in the cortex is non-uniform, with some retinal regions, with overlapping folds, being over-represented and others, where the lattice points are further apart, relatively under-represented.

relatively over-represented, and others under-represented. While the reasons for this do not seem intuitively clear, calculations confirmed that substituting a uniform retinal map, i.e. one defined by $x_{i,j} = iX/(M - 1)$ and $yi,j = jY/(M - 1)$, for the non-uniform one, caused coverage values ($c'$) to increase, i.e. get worse. Thus a non-uniform retinotopic map can increase coverage uniformity.

## Discussion

In the Introduction, four questions were posed. (i) Are there limits on the number of continuous and periodic stimulus feature maps that can be overlaid so that all combinations of the different features occur with reasonably equal frequency? (ii) Does the structure of individual maps change as new maps are added? (iii) Do the structural relations between different maps change as new maps are added? (iv) If they do, is there any way one can tell, from looking at maps of individual features, how many additional features might be represented? Based on the simulations done here, the following answers to these questions can be given: (i) there does not appear to be a hard geometrical limit on the number of spatially periodic maps which can be overlaid, rather the ability to represent combinations of parameters degrades in a continuous way as increasing numbers of feature dimensions are added to the maps; (ii) the structure of individual maps does not change significantly as new maps are added; and (iii) although the structural relations between map pairs do change as new maps are added, (iv) these changes are relatively subtle and as a consequence it may not be easy to infer the presence or absence of additional maps by examining the structural relationships of those maps that are known to exist.

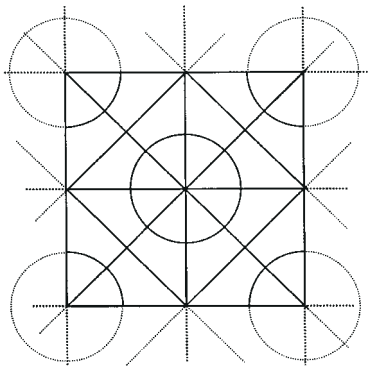

**Figure 8.** A construction which solves the coverage problem in a geometrically regular way for $N = 5$ although not for patterns of similar periodicity and morphology. Four of the protomaps are sets of parallel stripes, oriented 45° apart, and the fifth protomap is a set of circles on a cubic lattice. Solid lines demarcate 32 feature domains in a unit cell.

These conclusions might change if structurally different, and better, solutions to the mapping problem studied here could be demonstrated. Determining *the* optimum solution for each value of *N*, however, is likely to be a difficult, if not impossible, task. Although orthogonal sets of parallel unbranched stripes are probably the optimum solution for $N = 2$, geometrically simple solutions for arbitrarily large numbers of maps do not seem likely to exist, nor could it be assumed that the solutions were optimal if they did. For example, overlaying *N* sets of parallel stripes with staggered offsets = $\lambda/2N$ produces only $2N$ out of $2^N$ desired unique combinations. Sets of parallel stripes intersecting at angles of $180°/N$ solve the problem for $N = 2$ and $N = 3$, but larger values of *N* give irregular domain sizes, suggesting that parallel stripes are no longer the best arrangement. A construction which solves the problem for $N = 5$, for a combination of striped patterns and circular blobs with different spacings, is shown in Figure 8. It may be relevant that this possesses several of the features observed in the solutions produced by the Kohonen algorithm, including orthogonal intersections of pairs of boundaries, multiple crossings at single points, and regions subdivided by curved as well as straight lines (Fig. 3). Further subdivisions of this pattern, and related constructions, are possible, but only if patterns of increasing spatial frequency are used, which is a violation of the requirement that the patterns should have similar

morphologies. Solutions to this problem therefore seem likely in practise to be approximate and subject to soft rather than hard constraints on the number of dimensions and the extent to which they can be said to have solved the problem.

This point of view is supported by the results of the simulations done here which, based on the coverage criteria used to evaluate the solutions, do not point to an unambiguous limit on the maximum number of maps which can be overlaid. The first measure of coverage, $c'$ (eq. 7), which measures variability in the total 'response' of the cortex over a representative set of stimuli (which can vary in retinal position), increases by a factor of roughly 1.6 for each additional dimension. This is probably the most functionally relevant of the measures, but it is less directly related to the geometry of the feature domains (quite different map geometries might produce similar values), while what constitutes an acceptable upper limit to the measure is not clearly defined. The second measure, $c_2$, looks for circular 'holes' in the cortical representation of each possible feature combination, and ignores the retinotopic map as well as variability in the size of individual domains. The average value of $c_2$ increases linearly with the number of dimensions up to $N = 6$, and then increases at a faster rate. If an upper limit of $c_2 = 1$ is adopted (indicating the frequent presence of circular regions with a diameter equal to twice the protomap wavelength, within which specific feature combinations do not occur), then the maximum number of dimensions that can safely be represented is six.

One factor that may artefactually limit the achievement of uniform coverage in the simulations is the discrete representation of the cortical surface in the model. As $N$ increases, the average number of cortical pixels (array points) representing individual feature domains decreases, and so pixel variability in domain size may contribute to the non-uniformity of coverage. For example, for $N = 8$ the average domain size was about six pixels and some domains were only one or two pixels in size. However, a similar type of limit may apply to the real cortex, since the smallest unit available to represent a specific feature combination seems likely to be a 'minicolumn', which is usually defined (Mountcastle, 1978) as a thin column of cells ~30–50 μm in diameter running vertically from white matter to pia. If the protomaps all have a periodicity of 1 mm, and if it is assumed that the geometrical problem is solved so that all of the $2^N$ feature domains are represented within an area of 1 $mm^2$ and there is one feature domain per minicolumn, then the upper limit on $N$ would be nine (leading to a domain size of 44 μm) or ten (a domain size of 30 μm). If, as seems likely, domains get represented less frequently, then larger values of $N$ might be tolerated, although coverage uniformity would be correspondingly poor.

It is intuitively likely that the Kohonen algorithm used to generate the maps will produce arrangements that are close to optimal for coverage, given the competitive learning rule and the presentation of all possible stimuli with nearly equal frequency. However, although the algorithm does appear to produce good solutions, they are unlikely to be optimal for any of the specific coverage measures used here. One indication of this is that $c'$ tended to decrease, albeit very slowly, with continued stimulus presentations. However, it seemed unlikely that any of these changes would ever be large enough to obliterate the much larger effects of dimensionality. Variants of the algorithm, e.g. presenting fixed, equal numbers of different stimuli in random order, rather than with a uniform probability of occurrence (as was done here), might have resulted in better coverage, as might other algorithms, e.g. the elastic net algorithm (Durbin and Willshaw, 1987; Durbin and Mitchison, 1990). These possibilities have not so far been tested.

The possibility that the real cortex might produce better, and structurally different, solutions to the mapping problem posed here cannot be excluded. Such evidence as exists, however, points to similarities, rather than differences, between cortical maps, and the artificial ones studied here. In both cats (Hübener *et al.*, 1997) and monkeys (Obermayer and Blasdel, 1993) iso-orientation domain borders (which are equivalent to zero-crossings given a vector representation of orientation and an appropriately chosen coordinate system) tend to intersect ocular dominance borders (i.e. zero-crossings on the ocular dominance map) at right angles. Iso-orientation domain borders also tend to intersect spatial frequency column boundaries at right angles (Hübener *et al.*, 1997). Whether spatial frequency column borders tend to intersect ocular dominance column borders at right angles is not known; nor is it known whether the zero-crossings of the vector components of orientation maps themselves tend to intersect at right angles. If one assumes an equivalence between the intersection of a pair of zero-crossings, and an orientation singularity, then the tendency for these to occur in the centers of the ocular dominance columns in monkeys and in cats, as well as in the centers of the spatial frequency domains in the cat, is similar to the tendency observed here for the zero-crossing intersections to avoid each other as well as other zero-crossing boundaries. The observation of a tendency for the zero-crossings of three or more maps to coincide (i.e. short range attraction) has not yet been made experimentally. One manifestation of it would be a tendency for some orientation singularities to occur precisely on the borders of ocular dominance or spatial frequency domains, or at positions where these boundaries intersect. While singularities have been observed on the borders of ocular dominance stripes in the monkey (Bartfeld and Grinvald, 1992) and in the cat (Hübener *et al.*, 1997) it is not clear whether such placements occur more often than would be expected by chance. Finally, explicit calculations of coverage uniformity in combined orientation, ocular dominance and spatial frequency maps (N.V. Swindale *et al.*, submitted) suggest that the spatial configuration of the maps is at a local minimum for coverage uniformity.

An earlier analysis of structural factors affecting coverage uniformity (Swindale, 1991) showed that random superposition of maps with similar spatial periodicities leads to poor coverage. One of the findings of that study was that coverage could be improved significantly for random superpositions by making the periodicities of the maps different. Here, the simulations produced protomaps which had similar periodicities, and (as in Swindale's work) it has been shown that good coverage can be obtained for maps of similar periodicity, given appropriate structural relations between the different maps. These observations raise the possibility that further improvements in coverage, and in the maximum number of maps, could be obtained by relaxing the constraint that the maps have similar periodicities. Since real cortical protomaps do differ in periodicity this possibility is worth exploring further.

Finally, the present analysis has assumed as a constraint that the polymap must represent all possible combinations of binary feature variables with equal frequency over small regions of visual space. While this has the advantage of presenting the problem in a clear-cut way, the problem that is solved in most cortical maps in general seems likely to be different. Firstly, the stimulus values being represented may lie on a continuum, or be circular, as in the case of orientation, rather than binary.

Secondly, not all possible feature combinations may occur with equal frequency and so coverage should be measured relative to the frequency or probability of occurrence of the feature combination in question. Finally, some feature combinations may not occur at all because the combination is physically impossible, is not a property of the real world, has not been experienced yet, or is represented in some other map. In such cases one expects the protomaps to be overlaid in such a way that these combinations do not get represented. That the cortex is, in general, organized according to such principles seems plausible but remains to be demonstrated.

## Notes

I thank Graeme Mitchison for his comments on an earlier draft of this manuscript. The work was supported by a grant from NSERC of Canada.

Address correspondence to N.V. Swindale, Department of Ophthalmology, University of British Columbia, 2550 Willow Street, Vancouver, BC, Canada V5Z 3N9. Email: swindale@unixg.ubc.ca.

## References

Barlow HB, Blakemore CB, Pettigrew JD (1967) The neural mechanism of binocular depth discrimination. J Physiol 193:327–342.

Bartfeld E, Grinvald A (1992) Relationships between orientation-preference pinwheels, cytochrome oxidase blobs, and ocular dominance columns in primate striate cortex. Proc Natl Acad Sci USA 89:11905–11909.

Blasdel GG, Salama G (1986) Voltage sensitive dyes reveal a modular organization in monkey striate cortex. Nature 321:579–585.

DeAngelis, GC, Ghose GM, Ohzawa I, Freeman RD (1999) Functional micro-organization of primary visual cortex: receptive field analysis of nearby neurons. J Neurosci 19:4046–4064.

Dobbins A, Zucker SW, Cynader MS (1987) Endstopped neurons in the visual cortex as a substrate for determining curvature. Nature 329:438–439.

Durbin R, Willshaw DJ (1987) An analogue approach to the travelling salesman problem using an elastic net method. Nature 326:698–691.

Durbin R, Mitchison G (1990) A dimension reduction framework for understanding cortical maps. Nature 343:644–647.

Felleman D, Van Essen DC (1991) Distributed hierarchical processing in the primate cerebral cortex. Cereb Cortex 1:1–47.

Goodhill GJ (1993) Topography and ocular dominance: a model exploring positive correlations. Biol Cybernet 69:109–118.

Hubel DH, Wiesel TN (1974) Sequence regularity and geometry of orientation columns in the monkey striate cortex. J Comp Neurol 158:267–294.

Hubel DH, Wiesel TN (1977) Functional architecture of macaque monkey visual cortex. Proc R Soc Lond B 198:1–59.

Hubel DH, Wiesel TN, LeVay S (1977) Plasticity of ocular dominance columns in monkey striate cortex. Phil Trans R Soc Lond B 278: 131–163

Hübener M, Shoham D, Grinvald A, Bonhoeffer T (1997) Spatial relationships among three columnar systems in cat area 17. J Neurosci 17:9270–9284.

Kohonen T (1982) Self-organized formation of topologically correct feature maps. Biol Cybernet 43:59–69.

Kohonen T (1993) Physiological interpretation of the self-organizing map algorithm. Neural Networks 6:895–905.

Kohonen T, Hari R (1999) Where the abstract feature maps of the brain might come from. Trends Neurosci 22:135–139.

Landau P, Schwartz EL (1991) Computer simulation of cortical polymaps: a proto-column algorithm. Neural Networks 5:187–206.

Langner G, Sams M, Heil P, Schulze H (1997) Frequency and periodicity are represented in orthogonal maps in the human auditory cortex: evidence from magnetoencephalography. J Comp Physiol 181: 665–676.

Mountcastle VB (1978) In: The mindful brain (Schmitt FO, ed.), pp. 7–50. Cambridge, MA: MIT Press.

Nelson JI, Kato H, Bishop PO (1977) Discrimination of orientation and position disparities by binocularly activated neurons in cat striate cortex. J Neurophysiol 40:260–283.

Obermayer K, Blasdel GG (1993) Geometry of orientation and ocular dominance columns in monkey striate cortex. J Neurosci 13: 4114–4129.

Obermayer K, Ritter H, Schulten K (1990) A principle for the formation of the spatial structure of cortical feature maps. Proc Natl Acad Sci USA 87:8345–8349.

Obermayer K, Blasdel GG, Schulten K (1992) Statistical-mechanical analysis of self-organization and pattern formation during the development of visual maps. Phys Rev A 45:7568–7589.

Press WH, Teukolsky SA, Vetterling WT, Flannery BP (1994) Numerical recipes: the art of scientific computing, 2nd edn. Cambridge: Cambridge University Press.

Schreiner CE (1998) Spatial distribution of responses to simple and complex sounds in the primary auditory cortex. Audiol Neurootol 3:104–122.

Shmuel A, Grinvald A (1996) Functional organization for direction of motion and its relationship to orientation maps in area 18. J Neurosci 16:6945–6964.

Swindale NV (1991) Coverage and the design of striate cortex. Biol Cybernet 65:415–424.

Swindale NV, Bauer H-U (1998) Application of Kohonen's self-organizing feature map algorithm to cortical maps of orientation and direction preference. Proc R Soc Lond B 265:827–838.

Tanaka, S (1995) Topological analysis of point singularities in stimulus preference maps of the primary visual cortex. Proc R Soc Lond B 261:81–88.

Weliky M, Bosking WH, Fitzpatrick D (1996) A systematic map of direction preference in primary visual cortex. Nature 379:725–728.

Wolf F, Bauer, H-U, Geisel T (1994) Formation of field discontinuities and islands in visual cortical maps. Biol Cybernet 70:525–531.